Polarization Measurement of Cs Using the Pump Laser Beam

Rujie Li
Wei Quan
Jiancheng Fang
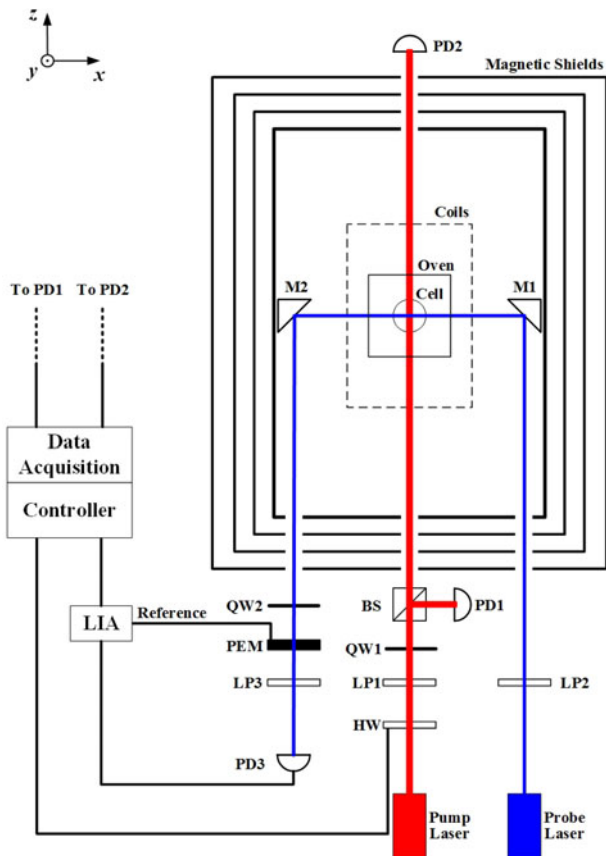
Polarization Measurement of Cs Using the Pump Laser Beam

Rujie Li ⓘ **, Wei Quan** ⓘ **, and Jiancheng Fang**

School of Instrument Science and Opto-electronics Engineering, Beihang University, Beijing 100191, China

Abstract: In the optically pumped systems, the spin polarization of the atoms is generally derived by employing additional modulations, in which way an extra perturbation will be introduced and thus affect the normal operation of the sensors. By investigating the absorption principle of the circularly polarized pump laser, here, we demonstrate the feasibility of extracting the electron-spin polarization from the transmitted intensity of the pump beam. This scheme can detect real-time polarization without disturbing the normal operation of the sensor, and the experimental result agrees well with the theory. This research is of value to the research and development of optically pumped systems, especially the magnetometer, and the comagnetometer operated in the spin-exchange relaxation free regime.

Index Terms: Atomic spin polarization, optical pumping, atomic magnetometer, field measurements.

1. Introduction

In optical pumping, absorption of the near-resonance circularly polarized light leads to large population imbalances in atomic ground states and induces the polarization of the atoms [1]. A variety of applications, from traditional studies on nuclear resonance gyroscope [2], atomic clock [3]–[5], optically pumped magnetometer [6]–[8] to the recently developed experiments in atomic spin gyroscope [9], [10], have utilized the electron-spin polarization for precise measurements. Among them, the recently developed spin-exchange relaxation free (SERF) magnetometer features a higher sensitivity and a much more portable package, compared to the superconducting quantum interference devices (SQUIDs), thus provides a better way to measure magnetocardiography (MCG) and magnetoencephalography (MEG) signals [11]–[13]. With a sufficiently high cell temperature and a weak residual magnetic field, such that $1/T_{se} \gg \omega_0$ (T_{se} is the time between spin-exchange collisions and ω_0 is the spin precession rate), the spin-exchange collisions would not broaden the magnetic resonance linewidth and it indicates the realization of the SERF regime [6]. As the operation principle of the sensors mentioned above relies on the spin polarization, the value of the polarization would affect the performance of these sensors. Thus, it is necessary to monitor the polarization of the alkali-metal atoms. A general experimental technique by turning the pump laser beam on and off has been used to calculate the spin polarization [14]. By applying an oscillating transverse

field and a strong longitudinal field, the electronic paramagnetic resonance (EPR) spectroscopy is another efficient method to obtain the population status [15], [16]. The previous schemes work very well for monitoring the spin polarization. However, to the best of our knowledge, the operation of optically pumped devices might have to be suspended due to the additional modulation applied for polarization measurements.

The motivation of this article is to develop a non-perturbative scheme to acquire the polarization of the electron-spin while minimizing the introduction of perturbation to the system. By investigating the relationship between the electron-spin polarization and the transmission of the circularly polarized pump laser beam, here we propose a new scheme, which only relies on the pump laser intensity, to extract the electron-spin polarization. Compared to the previous methods, this technique has the advantage that no extra disturbance is introduced into the sensor, and it also acts as a real-time method to monitor the electron-spin polarization. We experimentally validate the method in a SERF magnetometer and the results are in excellent agreement with the theory. From our perspective, this research is useful for the research and development of optically pumped systems, especially the magnetometer and the comagnetometer operated in the SERF regime.

2. Theoretical Model

The electron-spin polarization of the alkali-metal atoms along the z direction (pumping axis) P_z^e is defined by [17]

$$P_z^e = \frac{R_{op}}{R_{op} + R_{sd}}, \tag{1}$$

where R_{op} is the optical pumping rate due to the circularly polarized pump laser, R_{sd} is the spin-destruction rate due to collisions with other alkali atoms, buffer gas atoms and quenching gas molecules [18]. For a monochromatic laser, the optical pumping rate is described by

$$R_{op} = kI(z), \tag{2}$$

where k determined by the photo absorption cross-section as well as the waist of the laser beam is defined as the pumping rate per unit laser intensity [14], [15], z is the position in the cell and $I(z)$ is the corresponding laser intensity. The atoms illuminated by the pump laser will be polarized according to (1). Inserting (2) into (1), we arrive at the following expression for the spin polarization as a function of the laser intensity,

$$P_z^e = \frac{I(z)}{I(z) + 1/K}, \tag{3}$$

where the coefficient K is defined as $K = k/R_{sd}$. Note that (3) gives us the relationship between the electron-spin polarization and the laser intensity. If the value of K is known, then (3) provides a useful method to measure the atomic spin polarization.

As the pump beam with circular polarization propagates through the vapor cell, the the populations of the atoms are redistributed and the reduction in the laser intensity $I(z)$ is given by [19]

$$\frac{dI(z)}{dz} = -n\sigma(v)I(z)\left(1 - P_z^e\right), \tag{4}$$

where n is the density of the alkali vapor, $\sigma(v)$ is the absorption cross-section related to the laser frequency. According to (1), the spin polarization P_z^e is built up by increasing the intensity of the circularly polarized pump beam. For weak intensities, a nonlinear absorption arises due to the intensity-dependent term P_z^e in (4). Equation (4) can be solved via the Lambert W-function [20], and the solution is expressed as

$$I(z) = \frac{R_{sd}}{k} W\left(\frac{kI(0)}{R_{sd}} \exp\left(\frac{kI(0)}{R_{sd}} - n\sigma(v)z\right)\right), \tag{5}$$

where $W(z)$ satisfies the function $W(z)e^{W(z)} = z$, $I(0)$ and $kI(0)$ represent the incident laser intensity and the corresponding pumping rate. Equation (5) can be rewritten in a much more simplified form by replacing the term k/R_{sd} with K,

$$I(z) = \frac{1}{K} W\left(K I(0) \exp\left(K I(0) - O(z)\right)\right), \tag{6}$$

where $O(z) = n\sigma(\nu)z$ is the optical depth of the pump beam at position z [21]. Note that we can easily obtain the incident and transmitted laser intensities, $I(0)$ and $I(l)$, where l is the path length of the laser beam through the cell. The values of K as well as the optical depth $O(l)$ are the free parameters and can be obtained from the fit based on (6).

Substituting the values of K and the transmitted pump beam intensity $I(l)$, which can be monitored continuously, into (3), we can obtain the corresponding electron-spin polarization in real time. As (3) and (6) only rely on the intensity of the pump laser, thus the scheme for measuring the spin polarization proposed here can be conducted during the normal operation of the optically pumped devices.

A magnetic field B_y, which is applied perpendicular to the magnetic moment of the polarized atoms, will cause a torque on the atoms and induce the Larmor precession. The precession of the spin polarization P_z^e will result in a projection on x axis, indicated as P_x^e. For the ultra-sensitive SERF magnetometry, the component P_x^e is generally detected by a linearly polarized probe beam and the magnetic field response is expressed as [19],

$$P_x^e \approx \frac{P_z^e \gamma^e}{R_{op} + R_{sd}} B_y, \tag{7}$$

where P_x^e is the x-component of the spin polarization P_z^e and $\gamma^e = g_s\mu_B/\hbar$ is the gyromagnetic ratio of a bare electron. P_x^e can be detected via the optical rotation of the probe beam, given by [22]

$$\theta = \frac{\pi}{2} l n r_e c f P_x^e \sum_{F_g, F_e} B_{F_g, F_e} \text{Im}\left[V\left(\nu - \nu_{F_g, F_e}\right)\right], \tag{8}$$

where $r_e = e/(m_e c^2) = 2.818 \times 10^{-15}$ m is the classical electron radius (e and m_e are the electric charge and the mass of the electron), c is the speed of the light, f is the oscillation strength (roughly 1/3 for D_1 transition and 2/3 for D_2 transition), $V\left(\nu - \nu_{F_g, F_e}\right)$ is optical resonance lineshape of the probe beam with Voigt profile, ν is the frequency of the probe light and ν_{F_g, F_e} is the resonance frequency of the transition $F_g \rightarrow F_e$, B_{F_g, F_e} is the strength of the optical rotation arising from the individual hyperfine resonance $F_g \rightarrow F_e$ and $\sum B_{F_g, F_e} = 1$.

3. Experiment Details

The configuration of the experimental setup used is depicted in Fig. 1, and is centered around a spherical vapor cell with a diameter of 12 mm. The vapor cell contains a droplet of Cs metal, 50 Torr of N_2 gas and 500 Torr of ^{4}He gas. The N_2 prevents radiation trapping, while ^{4}He is included to reduce the diffusion effect to the cell walls. The cell is held in an oven heated to 100 °C with twisted-pair wires driven by AC current at 100 kHz. A set of four cylindrical layers of μ-metal magnetic shield encloses the cell and provides a shielding factor of 10^6 to quasi-static magnetic fields. The vapor cell is optically pumped by a circularly polarized pump beam originating from a distributed feedback (DFB) laser. The pump laser, with a spectral width of about 2 MHz, is tuned to the Cs D_1 resonance line and directs along the z axis. According to (5), the transmitted laser intensity $I(l)$ would vary with the different incident laser intensity. The incident and the transmitted laser intensities are recorded by two photodiodes (PD1 and PD2), simultaneously.

The probe laser beam, formed by another DFB system, is detuned by about 0.3 nm to the red side of the D_2 resonance line and propagates in the x axis. The first calcite polarizer (LP2) determines the initial linear polarization axis at 0°. Faraday rotation from the atoms rotates the polarization plane of the probe beam by an angle θ [18]. Then, a quarter waveplate (QW2) with one of its axes
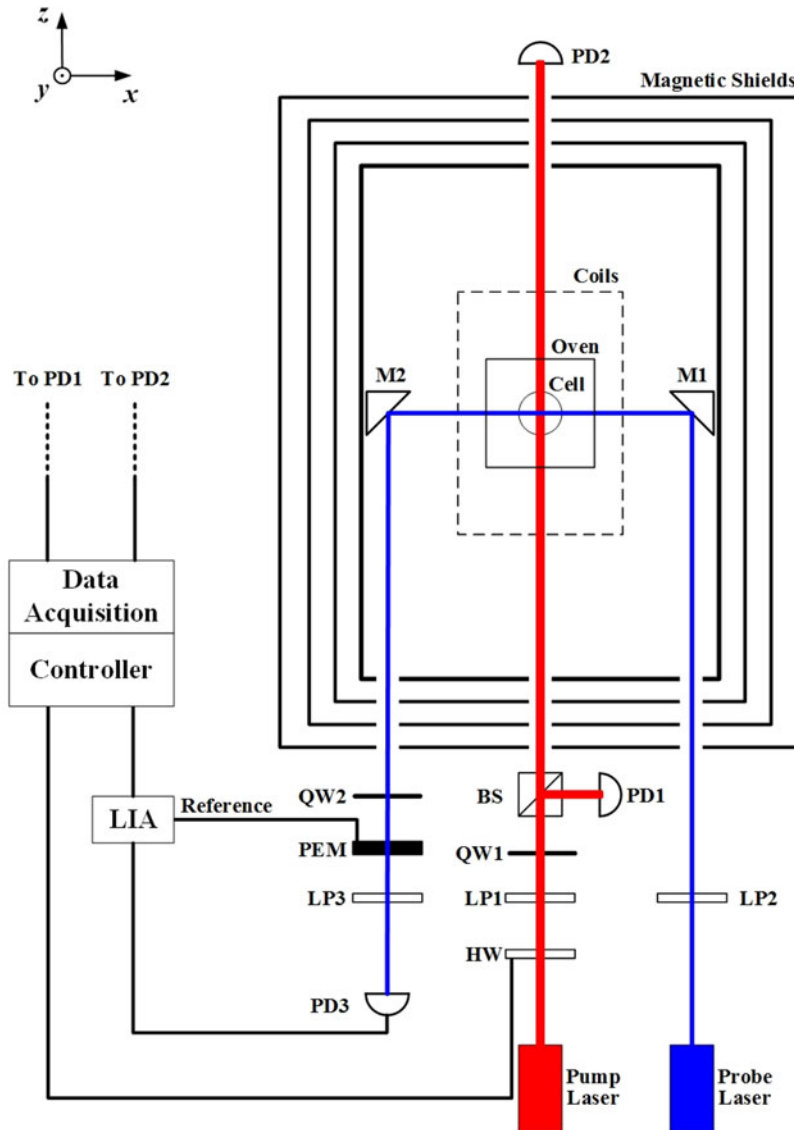
Fig. 1. Experimental setup. LP1, LP2 and LP3: linear polarizers, QW1 and QW2: quarter waveplates, BS: beam splitters, M1 and M2: reflection mirrors, PD1, PD2 and PD3: silicon photodiodes, PEM: photo-elastic modulator, LIA: lock-in amplifier. Red lines mark the pump laser path, while blue lines indicate the probe laser path. The HW also acts as an actuator and can be rotated by a stepper motor to stabilize the incident intensity of the cell.

nominally aligned with the calcite polarizer contributes a circular component proportional to θ. A final calcite polarizer (LP3), which acts as an analyzer and is crossed with the original polarizer, selects the time varying intensity of the transmitted light. A photo-elastic modulator (PEM) following the quarter waveplate is used to modulate the polarization of probe laser in order to improve the S/N (the ratio of signal to noise). And the modulation axis of the PEM is oriented at $45°$ with respect to the transmission axis of the polarizer [23]. Finally, the probe beam transmitted through the cell is detected by a photodiode (PD3) and the time-varying intensity on PD3 is given by [17]

$$I^P(t) \approx I_0^p \alpha \theta \sin(\omega t), \tag{9}$$

where I_0^p is the incident intensity of the probe beam, $\alpha \approx 0.08$ rad and $\omega \approx 50$ kHz are the modulation amplitude and modulation frequency of the PEM. Both the pump and probe beams have a circular
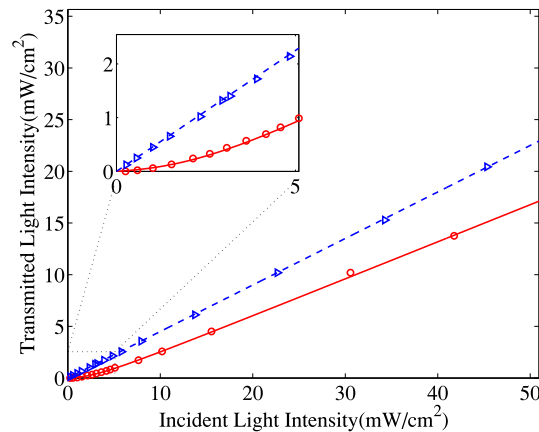
Fig. 2. The transmitted laser intensity as a function of the incident laser intensity of the circularly polarized pump beam. The blue triangles indicate the transmission of pump beam at the room temperature while the blue dashed line is the corresponding linear fitting curve. The red circles are obtained at 100 °C and the red line overlapping the data points is the fitting curve according to (6), from which the value of K is deduced. The inset shows magnification of the transmission curves.

cross-section with a diameter of 5 mm and the intensity mentioned here is the averaged laser power per unit area. In this case, only the relatively flat central part of the cell is illuminated to reduce the divergence caused by the cell. Note that the time-varying intensity of the probe beam $I^p(t)$ is definitely different from the distance-dependent intensity of the pump beam $I(z)$. The photocurrent express as (9) is amplified by a low-noise transimpedance amplifier and demodulated by a commercial computer-controlled digital lock-in amplifier (Zurich Instruments, model HF2LI) referenced to the PEM, from which the magnetic response is given. Via detecting the optical rotation of the polarization plane, the residual magnetic fields can be further canceled actively by three orthogonal coils inside the shields in order to realize the SERF regime. Under the SERF regime, the spin relaxation arising from the spin-exchange collisions is completely eliminated and the spin-destruction collisions dominate the absorption of the pump laser.

4. Results and Discussions

In Fig. 2, we plot the transmitted laser intensity as a function of the incident intensity at room temperature (25 °C) and 100 °C. The density of the vapor cell at room temperature is about $5.0 \times 10^{10} cm^{-3}$, more than two orders less than that at 100 °C ($n \approx 1.6 \times 10^{13} cm^{-3}$). At the room temperature, the incident intensity $I(0)$ is approximately equal to the transmitted intensity $I(l)$ in theory expressed by (6), where the systematic transmission has not been taken into account, thus the absorption due to atoms at 25 °C is negligible. The curve at room temperature in Fig. 2 is only used to measure the practical transmission of the cell and the related optics, which is necessary for the polarization measurements at high temperatures, while the trace at 100 °C is employed to calculate the spin polarization in the SERF regime. The incident and transmitted intensities of the pump laser beam shown in Fig. 2 are measured before and after the oven shown in Fig. 1. As the blue triangles shown in Fig. 2, the transmitted laser intensity at room temperature is proportional to the incident laser intensity. Note that the reduction in the laser intensity not only reflects the transmission of the cell, but it is also affected by the uncoated optical glass windows and focus lenses in the oven. Compared to the results obtained at room temperature, the data points at 100 °C show a nonlinear absorption when the incident intensity is less than about 5 mW/cm² (see inset in Fig. 2), from which the value of K is obtained via the curve fitting to (6). In our case K is 0.81 and $O(l)$ is 2.16, which agree reasonably with those calculated using the cell parameters. The value of K depends on a number of factors, including the cell pressure and the laser wavelength. At high laser intensities, the transmitted laser intensity $I(l)$ scales linearly with $I(0)$, which implies
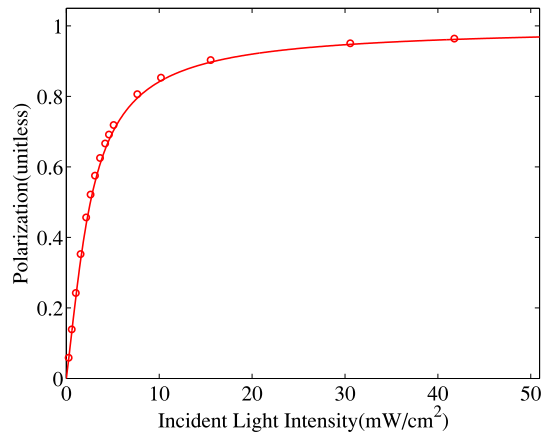
Fig. 3. The polarization of the alkali-metal atoms at the cell center as a function of the pump beam intensity. The red circles indicate the polarization of the alkali-metals deduced from the intensity of the circularly polarized pump laser based on (3), while the theoretical prediction according to (1) is marked by the red line. It should be known that (3) can be adopted to calculate the beam intensities at the cell center.

that the atoms are almost fully polarized. In theory, the two curves should be parallel to each other at high intensity. However, they feature different slopes in Fig. 2. The reason, what we believe, for this discrepancy is due to the undesirable linear component in the pump beam. The reduction in the linear component is much stronger than that in the circular component at 100 °C, while the absorptions of both linear and circular components are negligible at room temperature. In this way, the linear component appeared in the pump beam can decrease the slope of absorption curve at 100 °C. In our experiment, the degree of the pump beam polarization is approximately 0.9 and this factor has been included in the curve fitting process.

Using (3), we can achieve the polarization measurements with the laser intensity and the coefficient K obtained above. The electron-spin polarization of Cs atoms as a function of the incident laser intensity at 100 °C is shown in Fig. 3. When the incident light intensity of the pump beam is below 5 mW/cm^2, the spin polarization of Cs atoms rapidly increases with the light intensity. However, this trend slows down as the polarization approaches the equilibrium. The measured values based on (3) agree very well with the prediction described by (1), which verify the validity of the scheme proposed here.

The results of polarization measurements shown in Figs. 2 and 3 are based on the detection of the pump beam intensities, while the data plotted in Fig. 4 is the magnetic response extracted from the probe beam in the SERF magnetometer. During the measurement of the polarization, a step in the B_y field with an amplitude of 0.05 nT has been applied at each pump laser intensity in order to test whether the SERF magnetometer can operate well. A theoretical prediction by (8) has been shown in Fig. 4. In theory, a sharp peak should exist around the 50% polarization, where P_x^e expressed as (7) reaches a maximum, and the strength of magnetic response should decrease dramatically on both sides of the peak. The magnetic responses expressed as (9) are extracted by the lock-in amplifier and are marked by the hollow squares in Fig. 4. The magnetometer signal increases with the incident laser power in the range of 0∼1 mW. However, the response on the right side of 50% polarization decrease slowly, inconsistent with the the theory by (7). It is the result of diffusion of atoms into and out of the illuminated region at high pump intensities. As the diffusion atoms are free from the power broadening effect, their contribution to the rotation angle should also be accounted for, $P_{xd}^e \approx P_z^e \gamma^e B_y / R_{sd}$, where the term associated with the optical pumping rate has been dropped out compared to (7). As the red dashed line shown in Fig. 4, the fitting curve containing the diffusion effects fits the data better. This phenomenon has also been observed by Ledbetter *et al.* [24] The normal magnetic response of the SERF magnetometer in Fig. 4 demonstrates that the scheme can be conducted without affecting the operation of the sensor. Besides, the relationship between the
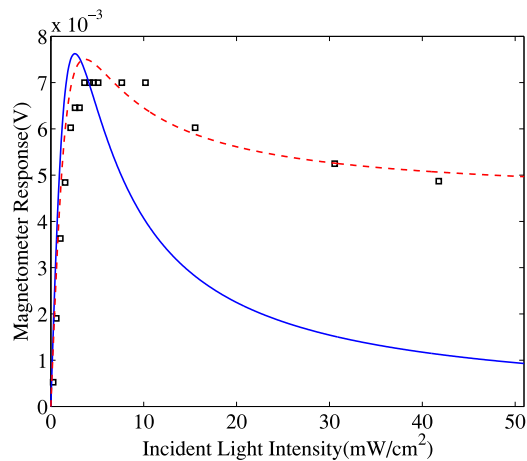
Fig. 4. The magnetometer responses as a function of the pump beam intensity. The black squares indicate the magnetometer response to a step magnetic field along y axis ($\triangle B_y \approx 50 pT$) at different pump laser intensity. This step field can result in a rotation angle of about 2.5×10^{-2} rad. The blue line shows the theoretical model in (8), while the red dashed line is the fitting curve in which the diffusion term has also been included.

magnetic response and the incident intensity, shown in Fig. 4, implies that the transmitted intensity can be used to control the power of the incident beam and thus the electron-spin polarization.

5. Conclusions

In summary, we have studied the relationship between the electron-spin polarization and the intensity of the circularly polarized pump laser, and a scheme for extracting the electron-spin polarization has been proposed. Compared to the previous methods, this technique mainly relies on the transmitted pump-laser intensity and operates in a non-perturbative mode. Therefore, the scheme described here can detect real-time polarization without disturbing the normal operation of the sensor. A comparison of the experimental results with theoretical calculations is also presented. The experimental results are in excellent agreement with the theoretical prediction. The corresponding magnetic field response of the SERF magnetometer as a function of the electron-spin polarization has also been investigated. And the diffusion term of atoms needs to be considered to explain the discrepancy at high pump intensities.

As the atomic spin polarization can be derived from the intensity of transmitted pump laser beam, the transmitted intensity can be used as the feedback signal to control the power of the incident beam and thus keep the electron-spin polarization stable. Compared to the traditional intensity-stabilization systems based on BS [23], [25], this strategy allows to reduce the number of optic components. From our perspective, this research is of value to the research and development of optically pumped systems, especially the magnetometer and the comagnetometer operated in the SERF regime.

References

[1] W. Happer, "Optical pumping," *Rev. Mod. Phys.*, vol. 44, pp. 169–249, 1972.
[2] K. F. Woodman, P. W. Franks, and M. D. Richards, "The nuclear magnetic resonance gyroscope: A Review," *J. Navigat.*, vol. 40, pp. 366–384, 1987.
[3] J. Camparo, J. Coffer, and J. Townsend, "Laser-pumped atomic clock exploiting pressure-broadened optical transitions," *J. Opt. Soc. Amer. B*, vol. 22, pp. 521–528, 2005.
[4] S. Knappe *et al.*, "A chip-scale atomic clock based on [87]Rb with improved frequency stability," *Opt. Express*, vol. 13, pp. 1249–1253, 2005.
[5] X. Zhang *et al.*, "Study on the clock-transition spectrum of cold [171]Yb ytterbium atoms," *Laser Phys. Lett.*, vol. 12, 2015, Art. no. 025501.

[6] J. C. Allred, R. N. Lyman, T. W. Kornack, and M. V. Romalis, "High-sensitivity atomic magnetometer unaffected by spin-exchange relaxation," *Phys. Rev. Lett.*, vol. 89, 2002, Art. no. 13080.

[7] A. Gusarov, D. Levron, E. Paperno, R. Shuker, and A. Ben-Amar Baranga, "Three-dimensional magnetic field measurements in a single SERF atomic-magnetometer cell," *IEEE Trans. Magn.*, vol. 45, no. 10, pp. 4478–4481, Oct. 2009.

[8] Z. D. Grujić, P. A. Koss, G. Bison, and A. Weis, "A sensitive and accurate atomic magnetometer based on free spin precession," *Eur. Phys. J. D*, vol. 69, p. 135, 2015.

[9] J. Fang, J. Qin, S. Wan, Y. Chen, and R. Li, "Atomic spin gyroscope based on ^{129}Xe-Cs comagnetometer," *Chin. Sci. Bull.*, vol. 58, pp. 1512–1515, 2013.

[10] R. Li, W. Fan, L. Jiang, L. Duan, W. Quan, and J. Fang, "Rotation sensing using a K-Rb-^{21}Ne comagnetometer," *Phys. Rev. A*, vol. 94, 2016, Art. no. 032109.

[11] K. Kim *et al.*, "Multi-channel atomic magnetometer for magnetoencephalography: A configuration study," *NeuroImage*, vol. 89, pp. 143–151, 2014.

[12] C. Johnson, P. D. D. Schwindt, and M. Weisend, "Magnetoencephalography with a two-color pump-probe, fiber-coupled atomic magnetometer," *Appl. Phys. Lett.*, vol. 97, 2010, Art. no. 243703.

[13] S. Taue, Y. Sugihara, T. Kobayashi, S. Ichihara, K. Ishikawa, and N. Mizutani, "Development of a highly sensitive optically pumped atomic magnetometer for biomagnetic field measurements: a phantom study," *IEEE Trans. Magn.*, vol. 46, no. 9, pp. 3635–3638, Sep. 2010.

[14] B. Lancor, E. Babcock, R. Wyllie, and T. G. Walker, "Circular dichroism of RbHe and RbN$_2$ molecules," *Phys. Rev. A*, vol. 82, 2010, Art. no. 043435.

[15] S. Appelt, A. Ben-Amar Baranga, C. J. Erickson, M. V. Romalis, A. R. Young, and W. Happer, "Theory of spin-exchange optical pumping of ^{3}He and ^{129}Xe," *Phys. Rev. A*, vol. 58, pp. 1412–1439, 1998.

[16] A. Ben-Amar Baranga, S. Appelt, C. J. Erickson, A. R. Young, and W. Happer, "Alkali-metal-atom polarization imaging in high-pressure optical-pumping cells," *Phys. Rev. A*, vol. 58, pp. 2282–2294, 1998.

[17] S. J. Seltzer, "Developments in alkali-metal atomic magnetometry," Ph.D. dissertation, Dept. Phy., Princeton Univ., Princeton, NJ, USA, 2008.

[18] J. Fang, R. Li, L. Duan, Y. Chen, and W. Quan, "Study of the operation temperature in the spin-exchange relaxation free magnetometer," *Rev. Sci. Instrum.*, vol. 86, 2015, Art. no. 073116.

[19] R. Wyllie, "The development of a multichannel atomic magnetometer array" Ph.D. dissertation, Dept. Phys., Univ. Wisconsin-Madison, Madison, WI, USA, 2012.

[20] C. Hwang and Y.-C. Cheng, "A note on the use of the Lambert W function in the stability analysis of time-delay systems," *Automatica*, vol. 41, pp. 1979–1985, 2005.

[21] A. Horsley, G.-X. Du, M. Pellaton, C. Affolderbach, G. Mileti, and P. Treutlein, "Imaging of relaxation times and microwave field strength in a microfabricated vapor cell," *Phys. Rev. A*, vol. 88, 2013, Art. no. 063407.

[22] S. J. Seltzer and M. V. Romalis, "High-temperature alkali vapor cells with antirelaxation surface coatings," *J. Appl. Phys.*, vol. 106, 2009, Art. no. 114905.

[23] L. Duan, J. Fang, R. Li, L. Jiang, M. Ding, and W. Wang, "Light intensity stabilization based on the second harmonic of the photoelastic modulator detection in the atomic magnetometer," *Opt. Express*, vol. 23, pp. 32481–32489, 2015.

[24] M. P. Ledbetter, I. M. Savukov, V. M. Acosta, D. Budker, and M. V. Romalis, "Spin-exchange-relaxation-free magnetometry with Cs vapor," *Phys. Rev. A*, vol. 77, 2008, Art. no. 033408.

[25] R. Li, Y. Li, L. Jiang, W. Quan, M. Ding, and J. Fang, "Pressure broadening and shift of K D_1 and D_2 lines in the presence of ^{3}He and ^{21}Ne," *Eur. Phys. J. D*, vol. 70, 2016, Art. no. 139.